Genistein regulates adipogenesis by blocking the function of adenine nucleotide translocase-2 in the mitochondria

Takahiro Ikeda[a], Shun Watanabe[a] and Takakazu Mitani[a,b,*]

[a]Division of Food Science and Biotechnology, Department of Agriculture, Graduated School of Science and Technology, Shinshu University, 8304 Minami-minowa, Kamiina, Nagano, 3994598, Japan;

[b]Division of Bioscience and Biotechnology, Faculty of Agriculture, Shinshu University, 8304 Minami-minowa, Kamiina, Nagano, 3994598, Japan

*To whom correspondence should be addressed: Takakazu Mitani, Tel.: +81-265-77-1608, Fax: +81-265-77-1315; E-mail: mitani@shinshu-u.ac.jp

Running title: Genistein-bound ANT2 suppresses adipogenesis

Abstract

Genistein exerts anti-adipogenic effects, but its target molecules remain unclear. Here, we delineated the molecular mechanism underlying the anti-adipogenic effect of genistein. A pulldown assay using genistein-immobilized beads identified adenine nucleotide translocase-2 as a genistein-binding protein in adipocytes. Adenine nucleotide translocase-2 exchanges ADP/ATP through the mitochondrial inner membrane. Similar to the knockdown of adenine nucleotide translocase-2, genistein treatment decreased ADP uptake into the mitochondria and ATP synthesis. Genistein treatment and adenine nucleotide translocase-2 knockdown suppressed adipogenesis and increased phosphorylation of AMP-activated protein kinase. Adenine nucleotide translocase-2 knockdown reduced the transcriptional activity of CCAAT/enhancer-binding protein β, whereas AMP-activated protein kinase inhibition restored the suppression of adipogenesis by adenine nucleotide translocase-2 knockdown. These results indicate that genistein interacts directly with adenine nucleotide translocase-2 to suppress its function. The downregulation of adenine nucleotide translocase-2 reduces the transcriptional activity of CCAAT/enhancer-binding protein β via activation of AMP-activated protein kinase, which consequently represses adipogenesis.

Key words: adipogenesis, AMPK, ANT2, genistein, target molecule

Graphical abstract caption

Genistein suppresses the ANT2 function by directly interaction. The dysfunction of ANT2 suppresses adipogenesis through activation of AMPK.

Obesity is a global health problem and affects more than 600 million adults and 100 million children worldwide (Ashkan *et al*. 2017). Obesity increases the incidence of diseases, including type 2 diabetes mellitus, cardiovascular disease, and cancer (O'Neill and O'Driscoll 2015). Excess hypertrophy (increase in the volume of adipocytes) and hyperplasia (excess formation of new adipocytes through differentiation of preadipocytes) of adipocytes in adipose tissues in response to a high-fat and -sugar diet contribute to the induction of obesity. Adipogenesis is the formation process of adipocyte from stem cells, and its process has two differentiation phases: commitment and terminal differentiation. Mesenchymal stem cells, including stromal cells, are converted into committed preadipocytes, which then differentiate into mature adipocytes (Cristancho and Lazar 2011). In mature adipocytes, energy from dietary sources is stored in the form of triacylglycerols (TAGs), and excessive TAG storage induces cell expansion, leading to adipocyte hypertrophy and obesity (Ghaben and Scherer 2019; Cristancho and Lazar 2011). Adipogenesis is a key process in determining the number of adipocytes, which mainly occurs during childhood and adolescence (Ghaben and Scherer 2019). Therefore, suppression of adipogenesis is an effective strategy for preventing obesity.

Adipogenesis is regulated by transcription factors such as peroxisome proliferator-activated receptor γ (PPARγ) and CCAAT/enhancer-binding protein (C/EBP) family members (Lefterova *et al*. 2008). PPARγ is the master regulator of adipogenesis and together with C/EBPα induces the expression of target genes such as *LIPIN1* (essential for lipid droplet formation) and *DGAT1/2* (encoding diacylglycerol acyltransferase, which is essential for TAG biosynthesis) (Festuccia *et al*. 2009). The enhancer region of the PPARγ gene (*PPARG*) contains C/EBP-binding sites, and *PPARG* expression is induced by C/EBPβ. C/EBPβ and C/EBPδ are early adipogenic transcription factors, and

63 their expression is induced immediately after stimulation with differentiation inducers.
64 The transcriptional activity of C/EBPβ is regulated by post-translational modifications
65 (Guo, Li, and Tang 2005). Phosphorylation of C/EBPβ causes dimerization of C/EBPβ,
66 and the dimer form binds directly to target genes, such as *PPARG* (Tang *et al*. 2005).
67 Overexpression of C/EBPβ lacking DNA-binding ability led to the suppression of PPARγ
68 protein expression and adipogenesis (Zhang *et al*. 2004).

69 Certain phytochemicals inhibit adipogenesis and high-fat diet-induced obesity. The
70 molecular mechanisms underlying the anti-adipogenic effects of phytochemicals are
71 diverse and include the induction of apoptosis and inhibition of the cell cycle via various
72 cell signaling pathways, including WNT/β-catenin signaling, mitogen-activated protein
73 kinase pathways, and the AMP-activated protein kinase (AMPK) pathway (Ahn *et al*.
74 2010; Kwon *et a*l. 2012; Liang *et al*. 2018). AMPK plays an important role in the
75 maintenance of cellular energy homeostasis (Hardie 2007). The functional activity of
76 AMPK requires phosphorylation at Thr172, which is induced by allosteric binding of
77 AMP due to a decrease in intracellular ATP (Hardie 2007). Although phytochemicals and
78 pathways that suppress adipogenesis have been well researched, for some phytochemicals,
79 the target molecules and mechanism of adipogenesis suppression remain unclear.

80 Genistein (4′,5,7-trihydroxyisoflavone) is an isoflavone that is more abundant than
81 daidzein and glycitein in soybeans and has a heterocyclic diphenolic structure similar to
82 that of estrogen (Adlercreutz *et al*. 1995). Genistein has various physiological activities,
83 and some studies have indicated that genistein exerts an anti-adipogenic effect. For
84 example, in 3T3-L1 adipocyte-like cells, it suppressed adipogenesis when used at high
85 concentrations (50–100 μM) (Harmon and Harp 2001; Hwang *et al*. 2005), while in
86 primary human adipocytes, it inhibited adipogenesis even at 6.25 μM (Park *et al*. 2009).

However, the target molecules involved in the anti-adipogenic effect of genistein remain unclear to date. In this study, we identified adenine nucleotide translocase-2 (ANT2) as a genistein-binding protein in adipocytes.

ANTs are integral membrane proteins inserted into the mitochondrial inner membrane that catalyze ATP transport from the mitochondrial matrix to the intermembrane space and ADP transport from the intermembrane space to the matrix (Brenner *et al*. 2011). Thus, they play an essential role in cellular energy metabolism. In addition, ANTs influence cell death by interacting with pro-apoptotic proteins and are required for mitochondrial degradation by mitophagy in several cell types (Hoshino *et al*. 2019). ANTs occur in four isoforms (ANT1–4) that are expressed in a tissue-specific manner. ANT1 is highly expressed in skeletal and cardiac muscles, whereas ANT2 is widely expressed in all somatic tissues (Brenner *et al*. 2011). We investigated the effect of genistein on ANT2 function in adipocytes and determined the role of ANT2 in adipogenesis. Similar to knockdown of ANT2, genistein treatment decreased ADP uptake into the mitochondria *in vitro*. Knockdown of ANT2 decreased TAG accumulation in primary adipocytes and increased AMPK phosphorylation. Furthermore, we demonstrated that genistein-inhibited ANT2 function suppressed adipogenesis by inhibiting the transcriptional activity of C/EBPβ via AMPK activation.

Materials and Methods

Plasmids

The cNDA encoding mouse *Ant2* (GenBank accession no. NM_007451) was amplified by PCR using mouse adipose tissue cDNA and subcloned into pLVSIN-Myc, termed by

pLVSIN-Myc-ANT2, respectively. The *Ant2* cNDA subcloned into pET-30a(+) vector, yield a ANT2 expression vector with six tandem N-terminal His-tags (pET-30a-ANT2). The Ant2 mutant cDNA encoding a siRNA-resistant form of ANT2, designed ANT2(mut), was synthesized by site-directed mutagenesis of *Ant2* cDNA using mutation primers, 5′-TTtAAgGAcAAgTAtAAaCAG-3′ and 5′-TGtTTaTAcTTgTCcTTaAAtGCAAA-3′ (lower-case letters indicate mutation sites), followed by construction of pLVSIN-Myc-ANT2(mut). The mouse C/EBPβ protein expression vector (pLVSIN-Myc-C/EBPβ) has been described previously (Mitani *et al*. 2020). A C/EBP-responsive reporter plasmid (pC/EBP-RE-Luc) was constructed. Four C/EBP response elements (C/EBP-RE: 5′-ATGGCGAGAAAATGACGAATGATGGCGAGAACCTGACGAAAT-3′) were inserted into the pGL4.14 vector (Promega, Madison, WA, USA). pBABE-puro SV40 LT was a gift from Thomas Roberts (#13970, Addgene, Cambridge, MA, USA), and the lentivirus expression vector of simian virus 40 large T antigen (SV40 LT) was constructed by subcloning SV40 LT cDNA into pBABE-puro SV40 LT into the pLVSIN vector. Mouse *Esr1* (GenBank accession no. NM_001302531; protein name is ERα) cDNA was amplified by PCR using mouse adipose tissue cDNA and subcloned into pLVSIN-Myc, termed pLVSIN-Myc-ERα. An ER-responsive reporter vector (pERE-Luc) was constructed. Four ER-responsive elements (ERE: 5′-GTCACTGTGACCAAGGTCACTGTGACCAAGGTCACTGTGACCAAGGTCACT GTGACC-3′) were inserted into the pGL4.10 vector (Promega).

Cell culture

Primary adipose stromal cells (ASCs) were isolated from inguinal adipose tissues of 3–4-week-old mice (Shizuoka, Japan). Animal experiments were performed conforming to the protocols approved by the Institutional Animal Care and Use Committee of Shinshu University Animal in accordance with Experimentation Regulations (Permission Number 019024) and the Guide for Care and Use of Laboratory Animals (NIH Publications No. 8023, revised 1978). Collected tissues were minced and incubated with 0.2% collagenase type II in isolation buffer (100 mM HEPES-NaOH, pH 7.4 containing 123 mM NaCl, 5 mM KCl, 1.3 mM $CaCl_2$, 5 mM glucose, and 4% BSA) at 37 °C for 1 h. The cell suspension was filtered through a 100-μm filter and placed on ice for 30 min. The suspension was filtered through a 40-μm filter to remove the remaining mature adipocytes. ASCs were pelleted by centrifugation at 700 × *g* for 10 min and suspended in Dulbecco's modified Eagle's medium with a high concentration of glucose (4.5 g/L) (DMEM-HG). After centrifugation at 700 × *g* for 10 min, the pelleted cells were resuspended in DMEM supplemented with 20% FBS, 10 mM HEPES, 100 units/mL penicillin, and 100 μg/mL streptomycin (+P/S). ASCs were infected with a lentivirus expressing a large T antigen (pLVSIN-SV40 LT), and immortalized ASCs were selected using puromycin (2 μg/mL). Confluent ASCs were induced to differentiate into adipocytes using an adipocyte differentiation cocktail (1 μM dexamethasone, 0.5 mM 3-isobutyl-1-ethylxanthine, 10 μg/mL insulin), 5 μM rosiglitazone, and 8 ng/mL biotin in DMEM-HG (+10% FBS, +P/S) for the first two days. Then, the cells were cultured in the same medium with insulin and biotin for another five days. The medium was changed every two days. Murine 3T3-L1 cells were purchased from the Japanese Collection of Research Bioresources (IFO050416), and the cells underwent a pre-adipose to adipose-like conversion. The culture and adipocyte differentiation methods used have been described previously

158 (Mitani *et al*. 2017). HEK293FT cells were purchased from Takara Bio and were cultured
159 in DMEM-HG (+10% FBS, +P/S).
160
161 **siRNA treatment**
162 An siRNA directed against *Ant2* (siANT2) was designed using the siDirect software
163 version 2.0 (Naito *et al*. 2009) and was produced at Sigma-Aldrich (St. Louis, MO, USA).
164 The target sequence for the ANT2 siRNA duplex was 5′-
165 TGCCTTCAAAGATAAATACAAGC-3′. A control siRNA (siCTL) was also purchased
166 from Sigma-Aldrich (MISSION siRNA Universal Negative Control#1). The siRNA
167 duplexes (20 nM) were transfected into ASCs or 3T3-L1 cells in Opti-MEM using
168 Lipofectamine RNAiMAX reagent (Invitrogen, Carlsbad, CA, USA) according to the
169 manufacturer's protocol for 24 h.
170
171 **Identification of genistein-binding proteins**
172 For the preparation of genistein-immobilized beads (referred to as Gen-beads hereafter),
173 magnetic FG beads with epoxy linkers (0.5 mg; Tamagawa Seiki, Nagano, Japan) were
174 mixed with genistein in N,N-dimethylformamide at 60 °C for 16 h. Then, the beads were
175 washed twice with N,N-dimethylformamide and distilled water. Differentiated ASCs
176 were lysed in lysis buffer (20 mM HEPES-NaOH, pH 7.9, containing 100 mM KCl, 1
177 mM $MgCl_2$, 0.2 mM $CaCl_2$, 0.2 mM EDTA, 10% (v/v) glycerol, 0.1% (w/v) Nonidet P-
178 40, 1 mM dithiothreitol, and 0.2 mM phenylmethylsulfonyl fluoride) and centrifuged at
179 22,260 × *g* at 4 °C for 30 min. The supernatant was used as the cell lysate. The cell lysates
180 (200 μg protein) were incubated with Gen-beads or plain beads (control) (0.5 mg each) at
181 4 °C for 4 h, and then, the beads were washed with wash buffer (20 mM HEPES-NaOH,

pH 7.9, containing 1 M KCl, 1 mM $MgCl_2$, 0.2 mM $CaCl_2$, 0.2 mM EDTA, 10% (v/v) glycerol, 0.1% (w/v) Nonidet P-40, 1 mM dithiothreitol, and 0.2 mM phenylmethylsulfonyl fluoride) five times. Bead-bound proteins were subjected to SDS-PAGE followed by silver staining. Selected gel bands were subjected to in-gel digestion using trypsin (MS grade; Promega). Sample analysis, data processing, and protein identification were conducted by the Research Center for Supports to Advanced Science, Shinshu University, using previously described methods (Hiroki *et al*. 2018). Trypsin-digested peptides were loaded onto a nanoACQUITY ultra performance liquid chromatography Xevo quadrupole time-of-flight mass spectrometer (Q-TOF/MS; Waters, Milford, MA, USA), and mass spectrometry analysis was performed using nanoLC coupled by a nanoESI emitter to a Q-TOF/MS (Waters). Peptide data were collected by MassLynx (ver. 4.1; Waters) and processed with ProteinLynx Global server software (ver. 2.5.2; Waters). The processed peptide data were searched against a mouse protein database in Uniprot (www.uniprot.org).

Pulldown of genistein-bound proteins

ASC or 3T3-L1 cell lysates were incubated with Gen-beads at 4 °C for 4 h, and then, the beads were washed with wash buffer. To detect the interaction of recombinant ANT2 with Gen-beads, the pET-30a-ANT2 vector encoding His-tagged mouse ANT2 was transformed into *Escherichia coli* strain BL21 Star (DE3; Stratagene, La Jolla, CA, USA), and the N-terminal His-tagged recombinant ANT2 was purified using Ni Sepharose 6 Fast Flow (GE Healthcare, Madison, WI, USA). Recombinant His-tagged ANT2 was incubated with Gen-beads at 4 °C for 4 h. Bead-bound proteins were eluted in SDS buffer

at 98 °C for 5 min and subjected to SDS-PAGE, followed by western blotting using an anti-ANT2 antibody and anti-His-tag antibody.

ADP uptake assay

Mitochondria were prepared as previously described (Cho *et al*. 2017), with minor modifications. Briefly, ASCs were homogenized in IBc buffer (30 mM Tris-HCl, pH 7.4 containing 225 mM mannitol and 75 mM sucrose). The homogenate was centrifuged at 600 × *g* for 5 min, and the supernatant was centrifuged at 7,000 × *g* for 10 min. The pellets were washed twice with IBc buffer and suspended in respiration buffer (3 mM HEPES-NaOH, pH 7.4, containing 120 mM KCl, 5 mM KH_2PO4, and 20 mM $MgCl_2$). Mitochondria (4 μg) in the respiration buffer were incubated with 100 pmol ADP for 120 s. The reaction solution was centrifuged at 10,000 × *g* for 1 min, and the amount of ADP in the supernatant was measured using the ADP-Glo Kinase assay (Promega).

Measurement of intracellular ATP

Cells were treated with siANT2 or siCTL for 24 h. Then, the cells were incubated with or without genistein in the presence or absence of adipocyte differentiation cocktail for 24 h. Intracellular ATP was measured by chemiluminescence using the CellTiter-Glo 2.0 Assay (Promega).

Oil Red O staining

Differentiated ASCs were fixed with 4% paraformaldehyde, and intracellular TAGs were stained with Oil Red O solution (0.5% w/v) at 22 °C for 20 min. Then, the dye was

extracted with Triton X-100 (4% w/v) in isopropanol at 22 °C for 10 min. The absorbance of the extracted dye at 492 nm was measured.

Western blotting

Western blotting was performed as previously described (Mitani *et al*. 2017). Cell lysates were analyzed by western blotting using the following primary antibodies: mouse monoclonal antibodies anti-PPARγ [Clone; E-8], anti-β-actin [Clone; C4], and anti-C/EBPα [Clone; D-5] from Santa Cruz Biotechnology (Santa Cruz, CA, USA); anti-GAPDH [Clone; 6C5] from Nacalai Tesque (Kyoto, Japan), and anti-His-tag [Clone; OGHis] from MBL (Nagoya, Japan); rabbit polyclonal antibodies [anti-C/EBPδ from Santa Cruz Biotechnology; anti-C/EBPβ from Betyl Laboratories; anti-AMPK and anti-p-AMPK (Thr172) from Cell Signaling Technology (Beverly, CA, USA), and anti-ANT2 from ABclonal (Wuhan, China)]. After incubation with HRP-conjugated secondary antibodies, immunoreactive bands were detected using an LAS500 instrument (GE Healthcare).

Quantitative reverse transcription PCR (qPCR)

Total RNA was extracted from cells using Sepasol-RNA I Super G (Nacalai Tesque). cDNA was synthesized using ReverTra Ace. qPCRs were run using KAPA SYBR Green Master Mix (NIPPON Genetics, Tokyo, Japan) and the primers listed in Supplementary Table 1. Relative target gene expression levels were normalized to the expression of *Rn18S* (18S rRNA) as an endogenous control.

Luciferase reporter assay

3T3-L1 cells were transfected with reporter vectors [pC/EBP-RE-Luc or pGL4-ERE-Luc, and pRL-SV40 or pRL-TK (control reporter vector; Promega)] using Lipofectamine 3000 (Thermo Fisher Scientific) for 24 h. Then, the cells were incubated with compound C (5 μM) in the presence or absence of adipocyte differentiation cocktail for 24 h. Firefly and *Renilla* luciferase activities were measured using a GloMax 20/20 luminometer (Promega). The transfection efficiency was normalized to *Renilla* luciferase activity. Data are expressed as relative light units (RLU), calculated as firefly luciferase activity divided by *Renilla* luciferase activity.

Immunofluorescence microscopy

ASCs were cultured to confluence on cover glasses and then transfected with siANT2 or siCTL for 24 h. After transfection, the cells were incubated with or without 10 μM genistein in the presence of adipocyte differentiation cocktail for 12 h. Immunofluorescence microscopy was performed as described previously (Tanaka *et al*. in press). Briefly, the cells were reacted with a primary antibody (anti-C/EBPβ) and then with Alexa Fluor 488-conjugated anti-rabbit IgG for 1 h. Nuclei were stained with 4′,6-diamidino-2-phenylindole (DAPI; 1 μg/mL) for 20 min. Then, the cells were visualized using a BX-2700TL fluorescence microscope (WRAYMER, Japan).

Chromatin immunoprecipitation (ChIP) assay

ASCs were transfected with siANT2 or siCTL for 24 h. Then, the cells were incubated with or without 10 μM genistein in the presence of a differentiation cocktail for 12 h. The ChIP assay was performed as described previously (Mitani *et al*. 2012). Briefly, cell lysates were reacted with rabbit polyclonal anti-C/EBPβ IgG or control rabbit IgG at 4 °C

overnight and then with 40 μL of protein G-Sepharose resin (50% slurry) at 4 °C for 1 h. The immunoprecipitated protein-DNA complexes were eluted at 65 °C for 6 h. The following primers were used for PCR: C/EBP-binding site in the *Pparg* enhancer, forward primer, 5′-TTCAGATGTGTGATTAGGAG-3′ and reverse primer, 5′-AGACTTGGTACATTACAAGG-3′.

Statistical analysis

Data are expressed as the mean ± SD and were analyzed by one- or two-way ANOVA followed by Tukey's or Dunnett's post-hoc test. Statistical analysis was performed using JMP statistical software version 11.2.0 (SAS Institute, Cary, NC, USA). Statistical significance was set at $p < 0.05$.

Results

Genistein binds to mitochondrial protein ANT2 in adipocytes

Gen-beads were prepared and incubated with whole-cell extracts from ASCs to purify genistein-interacting proteins (Figure 1a). We digested genistein-binding proteins into peptides and analyzed them using a Q-TOF/MS. Peptide sequences predicted by mass spectrometry were searched against a mouse protein database, and the peptide sequences were found to match those of ANT2 (Figure 1b). The sequence coverage was 44.6%, suggesting that genistein interacted with ANT2. We determined whether genistein interacts with ANT2 in adipocytes by a pull-down assay followed by western blotting using ANT2-specific antibodies. The results showed that genistein interacted with ANT2 in ASCs and 3T3-L1 cells (Figure 1c). To investigate whether ANT2 directly binds

genistein, we purified His-tagged recombinant ANT2 and incubated it with Gen-beads. As shown in Figure 1d, recombinant ANT2 was pulled down by the Gen-beads. These results indicated that genistein physically interacts with ANT2 in adipocytes.

Genistein blocks ANT2-mediated ADP/ATP transport in the mitochondria

ANT2 is a transporter that takes up cytosolic ADP into the mitochondrial matrix and excretes synthesized ATP into the intermembrane space and cytosol. We examined the effect of genistein on mitochondrial ADP uptake using mitochondria isolated from ASCs. The uptake activity was decreased in mitochondria from ANT2-knockdown ASCs (Figure 2a). When isolated mitochondria were treated with genistein, ADP uptake was also decreased. Genistein treatment had no effect on the amount of ANT2 protein, indicating that genistein treatment and knockdown of ANT2 had the same effect. We next investigated the effect of genistein on intracellular ATP levels in ASCs. Metformin, an inhibitor of ATP synthesis, reduced intracellular ATP levels. Likewise, ANT2 knockdown and genistein treatment reduced intracellular ATP levels (Figure 2b). These effects were also observed in 3T3-L1 adipocytes. These results suggested that genistein suppresses intracellular ATP synthesis by inhibiting ANT2 function.

Knockdown of ANT2 results in decreased lipid accumulation in ASCs

Genistein suppresses the function of ANT2; however, the function of ANT2 in adipogenesis is still unknown. We examined whether ANT2 is involved in TAG accumulation using Oil Red O staining. ANT2 knockdown reduced TAG accumulation in ASCs (Figure 3a). Genistein also reduced the amount of TAGs in ASCs at concentrations above 5 μM (Figure 3b). To determine whether ANT2 contributes to the

suppressive effect of genistein, we treated ANT2 siRNA-treated ASCs with genistein. Interestingly, genistein did not further reduce TAG accumulation in ANT2 siRNA-treated ASCs (Figure 3c), suggesting that the genistein-mediated anti-adipogenic effect is dependent on ANT2. Furthermore, we investigated the effect of *Ant2* knockdown on the gene expression of fatty acid synthesis-related enzymes. ANT2 knockdown suppressed the expression of *de novo* lipogenesis-related genes in ASCs (Figure 3d). These results demonstrated that ANT2 regulates adipogenesis at the gene expression level and that genistein exerts its anti-adipogenic effect through the suppression of ANT2.

Genistein treatment and ANT2 knockdown suppress adipocyte differentiation in the early phase

We examined ANT2 expression levels during the differentiation process. ANT2 protein expression was detected on day 1 after the start of differentiation and increased in a differentiation time-dependent manner (Figure 4a, *left panels*). Interestingly, the expression level of ANT1, which is a homolog of ANT2, decreased throughout the adipocyte differentiation process (Figure 4a, *right panel*). To investigate whether ANT2 knockdown and genistein suppress adipogenic differentiation and not merely reduce TAG accumulation, we analyzed the protein levels of transcription factors involved in adipocyte differentiation. ANT2 knockdown suppressed the protein levels of PPARγ and C/EBPα (Figure 4b). However, C/EBPβ and C/EBPδ protein expression was not affected by ANT2 knockdown (Figure 4c). Similar results were obtained in genistein-treated ASCs. These results indicated that genistein-mediated inhibition of ANT2 regulates adipogenesis and adipocyte differentiation in ASCs.

The estrogen receptor (ER) is not involved in the anti-adipogenic effect of genistein in ASCs

Genistein acts as a ligand for the ER, and estrogen suppresses adipocyte differentiation through ERα (Homma *et al*. 2000). In fact, genistein upregulated ERα-mediated transcriptional activity, which was inhibited by the ER antagonist, ICI182780 (Figure 5a). We determined whether genistein suppressed adipocyte differentiation through ERα using ICI182780. Genistein treatment partially reduced the protein levels of PPARγ and C/EBPα, even in the presence of ICI182780 (Figure 5b). These results indicated that the anti-adipogenic effect of genistein via inhibition of ANT2 function is a different pathway from the ERα pathway.

ANT2 knockdown attenuates the transcriptional activity of C/EBPs

ANT2 knockdown decreased PPARγ and C/EBPα protein levels but did not affect C/EBPβ and C/EBPδ protein levels. Therefore, we speculated that ANT2 is involved in the regulation of the transcriptional activity of C/EBPβ and C/EBPδ. To confirm this speculation, we performed a reporter assay using a luciferase vector containing C/EBP response elements. The transcriptional activity of C/EBPs was enhanced in cells incubated in adipocyte differentiation cocktail, and ANT2 knockdown downregulated C/EBP transactivation (Figure 6a, *left panel*). C/EBPβ rather than C/EBPδ plays a major role in adipogenesis (Tanaka *et al*. 1997). ANT2 knockdown also suppressed C/EBP transactivation in C/EBPβ-overexpressing cells (Figure 6a, *right panel*). To determine whether ANT2 is involved in C/EBP transactivation, ANT2(mut), which is an ANT2 siRNA-resistant form, was expressed. siANT2-suppressed C/EBP transactivation was restored upon expression of ANT2(mut) (Figure 6b). To determine whether ANT2

372 regulates the binding of C/EBPβ and DNA, a ChIP assay was performed using ANT2-
373 knockdown ASCs. ANT2 knockdown reduced the amount of C/EBPβ bound to the
374 enhancer region of *Pparg* (Figure 6c). Immunofluorescence microscopy showed that
375 C/EBPβ localized in the nucleus in ASCs and that its intracellular location was not
376 affected by ANT2 knockdown (Figure 6d, *left panels*). Similar results were obtained in
377 genistein-treated ASCs (Figure 6d, *right panels*). These results indicated that ANT2 is
378 involved in the modulation of the transcriptional activity of C/EBP by regulating the
379 association between C/EBPβ and its target DNA.
380
381 **Phosphorylation of AMPK is involved in ANT2knockdown-suppressed adipogenesis**
382 ANT2 knockdown and genistein treatment reduced intracellular ATP levels. Therefore,
383 we next examined whether ANT2-regulated ATP levels are involved in adipocyte
384 differentiation and C/EBP transactivation. ANT2 knockdown and genistein increased
385 AMPK phosphorylation on day 1 (Figure 7a). In contrast, on day 7, ANT2 knockdown
386 and genistein treatment suppressed AMPK phosphorylation. To determine whether
387 activated AMPK is involved in ANT2 knockdown-suppressed adipocyte differentiation,
388 ANT2-knockdown ASCs were incubated with compound C, an inhibitor of AMPK.
389 Compound C rescued the reduction in PPARγ protein levels induced by ANT2
390 knockdown or genistein treatment (Figure 7b and 7c). These results indicated that ANT2
391 promotes adipocyte differentiation by inhibiting AMPK activity.
392
393 **Blockade of AMPK phosphorylation cancels the effects of ANT2 knockdown**
394 Finally, we examined the effect of compound C on the transcriptional activity of C/EBPs
395 in ANT2-knockdown cells. Compound C elevated C/EBP transactivation and canceled

the ANT2-knockdown effect on C/EBP transactivation (Figure 8a). A ChIP assay showed that compound C suppressed the effect of ANT2 knockdown in reducing the amount of C/EBPβ bound to the *Pparg* enhancer region (Figure 8b, *upper panel*). Similarly, compound C restored the genistein-induced decrease in the amount of C/EBPβ-DNA complex (Figure 8b, *lower panel*). These results indicated that ANT2 elevated C/EBPβ transactivation by suppressing AMPK activity.

Discussion

Adipocyte hypertrophy due to excessive TAG accumulation can lead to type 2 diabetes mellitus, cardiovascular diseases, and cancer (Ghaben and Scherer 2019; Cristancho and Lazar 2011). The ingestion of dietary food factors is drawing attention as a strategy to prevent adipogenesis and adipocyte hypertrophy, and the anti-obesity effects of phytochemicals have been widely studied. However, only a few target molecules of phytochemicals have been identified. As a result, the detailed molecular mechanisms by which phytochemicals suppress adipogenesis have not been elucidated. In this study, we aimed to identify target proteins of the phytochemical genistein in adipocytes and to elucidate the molecular mechanism by which genistein exerts anti-adipogenic activity by binding to its target proteins. We identified ANT2 as a novel genistein-binding protein and demonstrated that genistein suppresses adipogenesis by inhibiting mitochondrial ANT2 function.

Knockdown of ANT2 decreased TAG accumulation and suppressed adipogenesis *in vitro*. Although the ANT1 and ANT2 isoforms have nearly 90% peptide sequence identity, they are localized to different compartments of the mitochondrial inner membrane and

420 are differentially involved in several cellular functions (Vyssokikh *et al*. 2001; Zamora *et*
421 *al*. 2004). ANT1 expression is repressed in cancer cells, and overexpression of ANT1
422 induces apoptosis in cancer cells (Zamora *et al*. 2004). In contrast, ANT2 expression is
423 increased in cancer cells, and ANT2 exerts an anti-apoptotic effect (Jang *et al*. 2008).
424 Moreover, ANT2 mediates fatty acid-induced uncoupled mitochondrial respiration,
425 whereas ANT1 is not found in brown adipose tissues (Shabalina *et al*. 2006). In this study,
426 ANT2 protein expression increased, whereas ANT1 expression decreased during
427 adipocyte differentiation of ASCs, indicating that increased ANT2 expression contributes
428 to the positive regulation of adipogenesis. Seo *et al*. (2019) reported a negative effect of
429 ANT2 on insulin resistance in obesity. Saturated fatty acids stimulate uncoupled
430 mitochondrial respiration in an ANT2-dependent manner, resulting in increased oxygen
431 consumption in adipose tissues. Increased oxygen consumption causes adipose tissue
432 inflammation and insulin resistance in obesity by increasing the levels of hypoxia-
433 inducible factor (HIF)-1α (Lee *et al*. 2014). Deletion of adipocyte ANT2 leads to the
434 suppression of inflammation accompanied with improved insulin resistance through
435 decreased HIF-1α protein levels in adipose tissue (Seo *et al*. 2019). Taken together, our
436 findings not only indicate that genistein treatment suppresses adipogenesis by interacting
437 with ANT2 but also suggest that it contributes to the improvement of insulin resistance
438 in obesity by inhibiting ANT2 function.
439 Genistein treatment decreased intracellular ATP levels and induced AMPK
440 phosphorylation in ASCs. Some studies have reported that food-derived factors such as
441 flavonoids and catechins induce AMPK activation, and food factors with an anti-
442 adipogenic effect are considered to exert their effect via AMPK activation (Liang *et al*.
443 2018; Choi *et al*. 2014). However, for some phytochemicals, it is not well known how

444 they lead to AMPK activation. An increase in the AMP/ATP or ADP/ATP ratio can be
445 caused by several factors, including the inhibition of mitochondrial ATP synthase,
446 inhibition of the respiratory chain, and decreased ADP uptake into mitochondria, which
447 results in increased AMP levels. 2-Deoxyglucose increases the ADP/ATP ratio by
448 inhibiting glycolysis and thus activating AMPK (Hawley *et al*. 2010). Quercetin inhibits
449 ATP synthase in purified mitochondria (Zheng and Ramirez 2000), and at high
450 concentrations (300 μM), it activates AMPK by decreasing oxygen uptake (Hawley *et al*.
451 2010). Although we did not examine the effect of genistein on the respiratory chain in
452 this study, our data suggest that, unlike 2-deoxyglucose and quercetin, genistein reduces
453 ATP production by suppressing mitochondrial ADP uptake. These results suggest that
454 genistein decreases ATP synthesis by blocking ANT2-mediated ADP/ATP translocation,
455 resulting in enhanced AMPK phosphorylation.
456 Genistein treatment and ANT2 knockdown induced AMPK phosphorylation in the
457 early phase but suppressed AMPK phosphorylation in the late phase of adipocyte
458 differentiation. The pharmacological AMPK activator 5-aminoimidazole-4-carboxamide
459 ribonucleoside (AICAR) inhibited adipogenesis in 3T3-L1 cells in the early phase of
460 adipocyte differentiation, and AICAR-treated diet-induced obese mice showed a
461 significant reduction in epididymal fat content (Habinowski and Witters 2001; Lee *et al*.
462 2011; Giri *et al*. 2006). However, contradictory results have been reported regarding
463 AMPK activation and adipogenesis. Compound C prevented the mitotic clonal expansion
464 of preadipocytes and subsequently blocked adipogenesis in 3T3-L1 cells (Gao *et al*. 2008).
465 The AMPK inhibitor BML-275 also suppressed adipogenesis in ischemia-challenged
466 human ASCs (Li *et al*. 2018). Gao *et al*. (2008) suggested that AMPK activation may
467 stimulate or suppress adipogenesis depending on the differentiation phase and that an

468 appropriate activation level of AMPK at the right time is essential for the induction of
469 adipocyte differentiation. AMPK activity is low in preadipocytes but gradually increases
470 three days after the initiation of differentiation (Giri *et al*. 2006), suggesting that AMPK
471 activation is important in the late phase of adipocyte differentiation and that AMPK
472 activity needs to be maintained at a low level in the early phase. Taken together, these
473 results indicate that genistein-mediated ANT2 inhibition suppresses adipogenesis via
474 AMPK activation in the early phase of adipocyte differentiation. Moreover, we showed
475 that compound C restored ANT2 knockdown-suppressed C/EBPβ transactivation,
476 suggesting that AMPK suppresses the transactivation of C/EBPβ.

477 AICAR suppresses PPARγ protein expression without affecting C/EBPβ protein levels
478 in 3T3-L1 cells (Giri *et al*. 2006; Lee *et al*. 2011). AMPK activation by AICAR enhances
479 β-catenin expression and nuclear accumulation (Wang and Di. 2015). β-Catenin acts as a
480 transcriptional coactivator in WNT/β-catenin signaling and indirectly suppresses the
481 transcriptional activity of PPARγ by inducing cyclin D1 and Myc (Fu *et al*. 2005). In
482 addition, some studies have reported that C/EBPβ activity negatively regulates WNT/β-
483 catenin signaling (Park *et al*. 2018; Guo *et al*. 2019), indicating that the suppression of
484 C/EBPβ activity leads to the upregulation of WNT/β-catenin signaling. Thus, our results
485 suggest that genistein- and ANT2 knockdown-activated AMPK downregulates
486 adipogenesis via two pathways, i.e., suppression of C/EBPβ activity and enhancement of
487 WNT/β-catenin signaling. However, it is unknown whether AMPK activation would
488 suppress C/EBPβ activity without affecting the protein level of C/EBPβ. Therefore, how
489 AMPK activation suppresses the transcriptional activity of C/EBPβ should be
490 investigated.

491 Genistein suppressed PPARγ and C/EBPα protein expression in the presence of the ER
492 antagonist ICI182780. Genistein is a heterocyclic phenol with structural similarity to
493 estrogens, and it regulates the transcriptional activity of ER by binding it in several cell
494 types (Adlercreutz *et al*. 1995). Estrogen inhibits body fat accumulation caused by a high-
495 fat diet by modulating the expression of genes regulating adipogenesis and lipolysis
496 (Stubbins *et al.* 2012; Jeong and Yoon 2011). Dietary genistein prevents denervation-
497 induced muscle atrophy, an effect that is canceled by ICI182780 (Aoyama *et al*. 2016).
498 Based on these findings, the majority of genistein-mediated beneficial effects have been
499 attributed to its estrogenic activity. However, the promoter activity and gene expression
500 of the β2-adrenergic receptor are increased by genistein but not by estradiol (estrogen) in
501 C2C12 myoblasts (Chikazawa and Sato 2018). Moreover, molecular docking studies have
502 shown that genistein interacts with c-Jun-NH_2-terminal kinase (JNK) and suppresses
503 TNF-α-mediated downregulation of adiponectin by inhibiting JNK in 3T3-L1 adipocytes
504 (Yanagisawa *et al*. 2012), indicating that genistein has multiple beneficial effects other
505 than those exerted through the ER. Our results demonstrate that genistein exerts an anti-
506 adipogenic effect not only through estrogenic activity but also through the new target
507 protein, ANT2, in adipocytes.
508 Genistein reduced lipid accumulation in ASCs at concentrations above 5 μM. In
509 previous in vivo studies, the plasma level of total genistein was increased to 18.0 ± 3.4
510 μM in rats orally administered genistein (40 mg/kg body weight) (Kwon *et al*. 2007). In
511 another study, the maximum serum level of total genistein was 7.68 ± 1.67 μM after the
512 administration of a single dose (20 mg/kg body weight) of a commercial supplement of
513 isoflavones via gavage (Sepehr *et al*. 2007). However, dietary genistein is mostly
514 metabolized to inactive conjugates, such as genistein-7-*O*-glucuronide, in the small

intestine and liver, resulting in low concentrations of circulating active aglycones (Gu *et al*. 2006; Zhen *et al*. 2012). In most studies comprising blood analyses, including the abovementioned studies, enzymatic hydrolysis using glucuronidase and sulfatase is used to process serum samples; consequently, the concentrations of genistein are presented as the sum of aglycone and conjugated genistein levels. Therefore, the concentration of circulating genistein aglycone is considered lower than 5 μM. However, glucuronidase activity in tissues may convert genistein conjugates into aglycones and consequently restore their health benefits, such as estrogenic activity. Macrophages at sites of inflammation exhibit high β-glucuronidase activity and convert flavonoid conjugates into aglycones (Terao *et al*. 2011; Galindo *et al*. 2012). Genistein-7-*O*-glucuronide activates macrophages and promotes the deconjugation of the glucuronide into aglycone in inflamed skin (Kaneko *et al*. 2017), suggesting that the concentration of genistein aglycone is higher in inflammatory tissues than in normal tissues. Adipose tissues in patients with obesity remain in a chronic low-grade inflammatory state, and the expanded adipocytes in these tissues secrete pro-inflammatory cytokines such as monocyte chemoattractant protein 1 (Ouchi *et al*. 2011). Monocyte chemoattractant protein 1 promotes bone marrow-derived monocyte infiltration into adipose tissues and induces the differentiation of monocytes into macrophages (Kanada *et al*. 2006). Thus, genistein conjugates might be deconjugated to genistein aglycone by macrophages present in the adipose tissues of patients with obesity, increasing genistein aglycone levels to concentrations that result in anti-adipogenic effects.

In summary, this study provided evidence that genistein suppresses adipogenesis by directly interacting with ANT2 and inhibiting its function in mitochondria. Although the anti-adipogenic effect of genistein has been previously investigated *in vitro* and *in vivo*,

539 this study for the first time revealed its target protein involved in its anti-adipogenic effect.
540 The suppression of ANT2 function results in reduced transcriptional activity of C/EBPβ
541 via AMPK activation, which leads to repressed adipogenesis. Thus, ANT2 may be a
542 therapeutic target for the prevention of obesity.
543

Acknowledgments

Protein detection, protein identification, and qPCR analysis were conducted at Research Center for Supports to Advanced Science, Shinshu University. We would like to thank Editage (www.editage.jp) for English language editing.

Funding

This work was supported by JSPS KAKENHI (grant number: 18K14405) for scientific research (to T.M.).

Data availability

The data of underlying this article will be shared on reasonable request to the corresponding author.

Author contributions

T.I. and T.M. conceived and designed the study. T.I. and T.M. performed the experiments. T.I., S.W., and T.M. interpreted the results. S.W. performed formal analysis. T.I. wrote the original draft. T.M. edited the original draft and wrote the manuscript.

Disclosure statement

No potential conflict of interest was reported by the authors.

564 **References**

565 Adlercreutz CH, Goldin BR, Gorbach SD *et al*. Soybean phytoestrogen intake and cancer
566 risk. *J Nutr* 1995;125:757S–70S.

567 Ahn J, Lee H, Kim S *et al*. Curcumin-induced suppression of adipogenic differentiation
568 is accompanied by activation of Wnt/beta-catenin signaling. *Am J Physiol Cell Physiol*
569 2010;298:C1510–6.

570 Aoyama S, Jia H, Nakazawa K *et al*. Dietary genistein prevents denervation-induced
571 muscle atrophy in male rodents via effects on estrogen receptor-α. *J Nutr*
572 2016;146:1147–54.

573 Ashkan A, Hohammad HF, Marissa BR *et al*. Health effects of overweight and obesity in
574 195 countries over 25 years. *N Engl J Med* 2017;377:13–27.

575 Brenner C, Subramaniam K, Pertuiset C *et al*. Adenine nucleotide translocase family:
576 four isoforms for apoptosis modulation in cancer. *Oncogene* 2011;30:883–95.

577 Chikazawa M, Sato R. Identification of a novel function of resveratrol and genistein as a
578 regulator of β2-adrenergic receptor expression in skeletal muscle cells and
579 characterization of promoter elements required for promoter activation. *Mol Nutr Food*
580 *Res* 2018;62:e1800530.

581 Cho J, Zhang Y, Park SY *et al*. Mitochondrial ATP transporter depletion protects mice
582 against liver steatosis and insulin resistance. *Nat Commun* 2017;8:14477.

583 Choi KM, Lee YS, Kim Wonkyun *et al*. Sulforaphane attenuates obesity by inhibiting
584 adipogenesis and activating the AMPK pathway in obese mice. *J Nutr Biochem*
585 2014;25:201–7.

586 Cristancho AG, Lazar MA. Forming functional fat: a growing understanding of adipocyte
587 differentiation. *Nat Rev Mol Cell Biol* 2011;12:722–34.

588 Festuccia W, Blanchard PG, Turcotte V *et al*. Depot-specific effects of the PPARγ agonist
589 rosiglitazone on adipose tissue glucose uptake and metabolism. *J Lipid Res*
590 2009;50:1185–94.
591 Fu M, Rao M, Bouras T *et al*. Cyclin D1 inhibits peroxisome proliferator-activated
592 receptor γ-mediated adipogenesis through histone deacetylase recruitment. *J Biol*
593 *Chem* 2005;280:16934–41.
594 Galindo P, Rodriguez-Gómez I, González-Manzano S et al. Glucuronidated quercetin
595 lowers blood pressure in spontaneously hypertensive rats via deconjugation. *PLoS One*
596 2012;7:e32673.
597 GaoY, Zhou Y, Xu A *et al*. Effects of an AMP-activated protein kinase inhibitor,
598 compound C, on adipogenic differentiation of 3T3-L1 cells. *Biol Pharm Bull*
599 2008;31:1716–22.
600 Ghaben AL, Scherer PE. Adipogenesis and metabolic health. *Nat Rev Mol Cell Biol*
601 2019;20:242–58.
602 Giri S, Rattan R, Haq E *et al*. AICAR inhibits adipocyte differentiation in 3T3L1 and
603 restores metabolic alterations in diet-induced obesity mice model. *Nutr Metab*
604 2006;3:31.
605 Gu L, House SE, Prior RL et al. Metabolic phenotype of isoflavones differ among female
606 rats, pigs, monkeys, and women. *J Nutr* 2006;136:1215-21.
607 Guo L, Guo YY, Li BY *et al*. Histone demethylase KDM5A is transactivated by the
608 transcription factor C/EBPβ and promotes preadipocyte differentiation by inhibiting
609 Wnt/β-catenin signaling. *J Biol Chem* 2019;294:9642–54.
610 Guo L, Li X, Tang QQ. Transcriptional regulation of adipocyte differentiation: a central
611 role for CCAAT/enhancer-binding protein (C/EBP) β. *J Biol Chem* 2015;290:755–61.

612 Habinowski SA, Witters LA. The effects of AICAR on adipocyte differentiation of 3T3-
613 L1 cells. *Biochem Biophys Res Commun* 2001;286:852–6.
614 Hardie DG. AMP-activated/SNF1 protein kinases: conserved guardians of cellular energy.
615 *Nat Rev Mol Cell Biol* 2007;8:774–85.
616 Harmon AW, Harp JB. Differential effects of flavonoids on 3T3-L1 adipogenesis and
617 lipolysis. *Am J Physiol Cell Physiol* 2001;280:C807–13.
618 Hawley S, Ross FA, Chevtzoff C *et al*. Use of cells expressing γ subunit variants to
619 identify diverse mechanisms of AMPK activation. *Cell Metab* 2010;11:554–65.
620 Hiroki M, Sawashita J, Ishikawa E et al. Comprehensive proteomic profiles of mouse
621 AApoAII amyloid fibrils provide insights into the involvement of lipoproteins in the
622 pathology of amyloidosis. *J Proteomics* 2018;172:111–21.
623 Homma H, Kurachi H, Nishio Y *et al*. Estrogen suppresses transcription of lipoprotein
624 lipase gene. Existence of a unique estrogen response element on the lipoprotein lipase
625 promoter. *J Biol Chem* 2000;275:11404–11.
626 Hoshino A, Wang WJ, Wada S *et al*. The ADP/ATP translocase drives mitophagy
627 independent of nucleotide exchange. *Nature* 2019;575:375–9.
628 Hwang JT, Park IJ, Shin JI *et al*. Genistein, EGCG, and capsaicin inhibit adipocyte
629 differentiation process via activating AMP-activated protein kinase. *Biochem Biophys*
630 *Res Commun* 2005;338:694–9.
631 Jang JY, Choi Y, Jeon YK *et al*. Suppression of adenine nucleotide translocase-2 by
632 vector-based siRNA in human breast cancer cells induces apoptosis and inhibits tumor
633 growth in vitro and in vivo. *Breast Cancer Res* 2008;10:R11.
634 Jeong S, Yoon M. 17β-Estradiol inhibition of PPARγ-induced adipogenesis and
635 adipocyte-specific gene expression. *Acta Pharmacol Sin* 2011;32:230–8.

636 Kanada H, Tateya S, Tamori Y et al. MCP-1 contributes to macrophage infiltration into
637 adipose tissue, insulin resistance, and hepatic steatosis in obesity. *J Clin Invest*
638 2006;116:1494-505.
639 Kaneko A, Matsumoto T, Matsubara Y et al. Glucuronides of phytoestrogen flavonoid
640 enhance macrophage function via conversion to aglycones by β-glucuronidase in
641 macrophages. *Immun Inflamm Dis* 2017;5:265-79.
642 Kwon JY, Seo SG, Heo YS *et al*. Piceatannol, natural polyphenolic stilbene, inhibits
643 adipogenesis via modulation of mitotic clonal expansion and insulin receptor-
644 dependent insulin signaling in early phase of differentiation. *J Biol Chem*
645 2012;287:11566–78.
646 Kwon SH, Kang MJ, Huh JS et al. Comparison of oral bioavailability of genistein and
647 genistein in rats. *Int J Pharm* 2007;337:148-54.
648 Lee H, Kang R, Bae S *et al*. AICAR, an activator of AMPK, inhibits adipogenesis via the
649 WNT/β-catenin pathway in 3T3-L1 adipocytes. *Int J Mol Med* 2011;28:65–71.
650 Lee YS, Kim JW, Osborne O *et al*. Increased adipocyte O_2 consumption triggers HIF-1α,
651 causing inflammation and insulin resistance in obesity. *Cell* 2014;157:1339–52.
652 Lefterova MI, Zhang Y, Steger DJ *et al*. PPARγ and C/EBP factors orchestrate adipocyte
653 biology via adjacent binding on a genome-wide scale. *Genes Dev* 2008;22:2941–52.
654 Li C, Chen K, Jia M *et al*. AMPK promotes survival and adipogenesis of ischemia-
655 challenged ADSCs in an autophagy-dependent manner. *Biochim Biophys Acta Mol*
656 *Cell Biol Lipids* 2018;1863:1498–510.
657 Liang Y, Sasaki I, Takeda Y *et al*. Benzyl isothiocyanate ameliorates lipid accumulation
658 in 3T3-L1 preadipocytes during adipocyte differentiation. *Biosci Biotechnol Biochem*
659 2018;82:2130–9.

660 Mitani T, Harada N, Nakano Y *et al*. Coordinated action of hypoxia-inducible factor-1α
661 and β-catenin in androgen receptor signaling. *J Biol Chem* 2012;287:33594–606.
662 Mitani T, Watanabe S, Wada K *et al*. Intracellular cAMP contents regulate NAMPT
663 expression via induction of C/EBPβ in adipocytes. *Biochem Biophys Res Commun*
664 2020;522:770–775.
665 Mitani T, Watanabe S, Yoshioka Y *et al*. Theobromine suppresses adipogenesis through
666 enhancement of CCAAT-enhancer-binding protein β degradation by adenosine
667 receptor A1. *Biochim Biophys Acta Mol Cell Res* 2017;1864:2438–48.
668 Naito Y, Yoshimura J, Morishita S *et al*. siDirect 2.0: updated software for designing
669 functional siRNA with reduced seed-dependent off-target effect. *BMC Bioinformatics*
670 2009;10:392.
671 O'Neill S, O'Driscoll L. Metabolic syndrome: a closer look at the growing epidemic and
672 its associated pathologies. *Obes Rev* 2015;16:1–12.
673 Ouchi N, Parker JL, Lugus JJ et al. Adipokines in inflammation and metabolic disease.
674 *Nat Rev Immunol* 2011;11:85-97.
675 Park HJ, Della-Fera MA, Hausman DB *et al*. Genistein inhibits differentiation of primary
676 human adipocytes. *J Nutr Biochem* 2009;20:140–8.
677 Park S, Lee MS, Gwak J *et al*. CCAAT/enhancer-binding protein-β functions as a
678 negative regulator of Wnt/β-catenin signaling through activation of AXIN1 gene
679 expression. *Cell Death Dis* 2018;9:1023.
680 Sepehr E, Cooke G, Robertson R et al. Bioavailability of soy isoflavones in rats Part I:
681 application of accurate methodology for studying the effects of gender and source of
682 isoflavones. *Mol Nutr Food Res* 2007;51:799-812.

683 Seo JB, Riopel M, Cabrales P *et al*. Knockdown of Ant2 reduces adipocyte hypoxia and
684 improves insulin resistance in obesity. *Nat Metab* 2019;1:86–97.
685 Shabalina IG, Kramarova TV, Nedergaard J *et al*. Carboxyatractyloside effects on brown-
686 fat mitochondria imply that the adenine nucleotide translocator isoforms ANT1 and
687 ANT2 may be responsible for basal and fatty-acid-induced uncoupling respectively.
688 *Biochem J* 2006;399:405–14.
689 Stubbins RE, Holcomb VB, Hong J *et al*. Estrogen modulates abdominal adiposity and
690 protects female mice from obesity and impaired glucose tolerance. *Eur J Nutr*
691 2012;51:861–70.
692 Tanaka E, Mitani T, Nakashima M *et al*. Theobromine enhances the conversion of white
693 adipocytes into beige adipocytes in a PPARγ activation-dependent manner. *J Nutr*
694 *Biochem* 2021, DOI:10.1016/j.jnutbio.2021.108898.
695 Tanaka T, Yoshida N, Kishimoto T *et al*. Defective adipocyte differentiation in mice
696 lacking the C/EBPβ and/or C/EBPδ gene. *EMBO J* 1997;16:7432–43.
697 Tang QQ, Grønborg M, Huang H *et al*. Sequential phosphorylation of CCAAT enhancer-
698 binding protein beta by MAPK and glycogen synthase kinase 3β is required for
699 adipogenesis. *Proc Natl Acad Sci U S A* 2005;102:9766–71.
700 Terao J, Murota K, Kawai Y. Conjugated quercetin glucuronides as bioactive metabolites
701 and precursors of aglycone in vivo. *Food Funct* 2011;2:11-7.
702 Vyssokikh MY, Katz A, Rueck A *et al*. Adenine nucleotide translocator isoforms 1 and
703 2 are differently distributed in the mitochondrial inner membrane and have distinct
704 affinities to cyclophilin D. *Biochem J* 2001;358:349–58.
705 Wang L, Di LJ. Wnt/β-Catenin mediates AICAR effect to increase GATA3 expression
706 and inhibit adipogenesis. *J Biol Chem* 2015;290:19458–68.

Yanagisawa M, Sugiya M, Iijima H *et al*. Genistein and daidzein, typical soy isoflavones, inhibit TNF-α-mediated downregulation of adiponectin expression via different mechanisms in 3T3-L1 adipocytes. *Mol Nutr Food Res* 2012;56:1783–93.

Zamora M, Meroño C, Viñas O *et al*. Recruitment of NF-κB into mitochondria is involved in adenine nucleotide translocase 1 (ANT1)-induced apoptosis. *J Biol Chem* 2004;279:38415–23.

Zhang JW, Tang QQ, Vinson C *et al*. Dominant-negative C/EBP disrupts mitotic clonal expansion and differentiation of 3T3-L1 preadipocytes. *Proc Natl Acad Sci U S A* 2004;101:43–7.

Zheng J, Ramirez VD. Inhibition of mitochondrial proton F0F1-ATPase/ATP synthase by polyphenolic phytochemicals. *Br J Pharmacol* 2000;130:1115–23.

Zhen Y, Kaustubh K, Wei Z *et al*. Bioavailability and pharmacokinetics of genistein: mechanistic studies on its ADME. *Anticancer Agents Med Chem* 2012;10:1264-80.

720 **Figure legends**

721 Figure 1. Genistein binds to adenine nucleotide translocase-2 (ANT2) in adipocytes. (a)
722 Genistein-binding proteins were purified from cell extracts of adipose stromal cells
723 (ASCs) using genistein-immobilized beads (+; Gen-bead) and detected by silver staining.
724 Gen-bead (−) indicates that beads without immobilized genistein, are used. Arrows
725 indicate a protein band that was identified by mass spectrometry analysis. (b) Amino acid
726 sequences of peptide fragments were obtained using nanoLC Q-TOF/MS, following
727 which the sequences were compared with those in a Uniprot mouse protein database. (c)
728 Pulldown assay using Gen-bead in adipose stromal cells (ASCs, *left panels*) and 3T3-L1
729 cells (*right panels*). The cell lysates were incubated with Gen-beads or control bead
730 followed by western blotting with anti-ANT2 and anti-β-actin antibodies. Gen-bead (−)
731 indicates that beads without immobilized genistein, are used. (d) Recombinant His-tagged
732 ANT2 was purified from *E. coli*, and then His-ANT2 and Gen-bead were incubated. Gen-
733 bead-bound protein was analyzed by western blotting with His-tag antibodies. Results are
734 representative of three independent triplicate experiments.
735
736 Figure 2. Genistein and ANT2 knockdown decreased intracellular ATP levels in
737 adipocytes. (a) ADP uptake capacity in mitochondria of ANT2-knocked down ASCs.
738 Isolated mitochondria were incubated with ADP (100 pmol) in the presence or absence
739 of genistein (Gen; 1 mM) for 120 sec. The amount of ADP in supernatant was measured.
740 (b) Intracellular ATP levels in ASCs (*left panel*) or 3T3-L1 cells (*right panel*) transfected
741 with ANT2 siRNA (siANT2; 20 nM) or control siRNA (siCTL). After transfection, the
742 cells were induced to adipocyte differentiation with differentiation inducer cocktail (DIC)
743 for 24 h. The cells were differentiated with DIC in the presence of Gen (10 μM) or

744 metformin (Metf; 1 mM) for 24 h. Data are expressed as means ± SD (n = 3). Statistically
745 significant differences are indicated by asterisk (*$p < 0.05$ vs. siCTL or veh). Results are
746 representative of three independent triplicate experiments.
747
748 Figure 3. Knockdown of ANT2 decreased lipid accumulation in ASCs. (a) Intracellular
749 lipid accumulation in ASCs transfected with siANT2 or siCTL. After siRNA transfection,
750 the cells were induced to adipocyte differentiation for 7 days. Left panels show oil red O-
751 staining. Scale bars indicate 50 μm. Right panel shows triacylglycerol (TAG) levels in
752 ASCs. (b) The accumulation of TAG in ASCs after induction of adipocyte differentiation
753 in the presence of the indicated concentrations of genistein (Gen). (c) TAG levels in ASCs
754 transfected with siANT2 or siCTL. After siRNA transfection, the cells were induced to
755 adipocyte differentiation in the presence or absence of 10 μM Gen. (d) qPCR analysis of
756 lipogenesis-related genes in ASCs treated with siANT2 or siCTL. After siRNA
757 transfection, the cells were induced to adipocyte differentiation. Data are expressed as
758 means ± SD (n = 3). In (a) and (d), statistically significant differences are indicated by
759 asterisks (*$p < 0.05$ vs. siCTL). In (b) and (c), statistically significant differences are
760 indicated by corresponding letters. If two groups share at least one letter between them,
761 the difference is not statistically significant. However, if two groups do not share any
762 letter, the difference between them is statistically significant. Results are representative
763 of three independent triplicate experiments.
764
765 Figure 4. Genistein and ANT2 knockdown suppressed adipogenesis at gene expression
766 levels. (a) Expression patters of ANT2 and other proteins in ASCs induced to adipocyte
767 differentiation. Left panels show protein expression. Right panel shows gene expression.

768 (b) Western blot analysis of adipocyte differentiation-associated proteins in ASCs. The
769 cells were transfected with siANT2, and then the cells were induced to adipocyte
770 differentiation in the presence or absence of 10 μM genistein (Gen) for 7 days (left panels).
771 (c) Protein expression of C/EBPs in ASCs. The cells were transfected with siANT2, and
772 then the cells were induced to adipocyte differentiation in the presence or absence of 10
773 μM Gen for 24 h. Data are expressed as means ± SD (n = 3). Results are representative
774 of three independent triplicate experiments.
775
776 Figure 5. Genistein suppressed adipogenesis even in the presence of ER antagonist. (a)
777 ERα-mediated transcriptional activity in ER antagonist ICI 182780 (1 μM; ICI) and Gen
778 (10 μM)-treated cells. (b) Western blot analysis of PPARγ and other proteins in ASCs.
779 The cells were induced to adipocyte differentiation with ICI 182780 (1 μM) in the
780 presence or absence of 10 μM Gen for 7 days. Data are expressed as means ± SD (n = 3).
781 Statistically significant differences are indicated by corresponding letters. If two groups
782 share at least one letter between them, the difference is not statistically significant.
783 However, if two groups do not share any letter, the difference between them is statistically
784 significant. Results are representative of three independent triplicate experiments.
785
786 Figure 6. Knockdown of ANT2 decreased transcriptional activity of C/EBPs. (a) C/EBP-
787 mediated transcriptional activity in 3T3-L1 adipocytes treated with siANT2 or siCTL.
788 siRNA-treated 3T3-L1 adipocytes were transiently transfected with a pC/EBP-RE-Luc
789 vector, followed by induction of differentiation with differentiation inducer cocktail
790 (DIC) for 24 h (*left panel*). The cells were transfected with C/EBPβ-expressing vector
791 (*right panel*). (b) C/EBP-mediated transcriptional activity in 3T3-L1 adipocytes or its

792 stable cell line expressing ANT2(mut) that is an siRNA-resistant form of ANT2. (c) ChIP
793 analysis in ASCs treated with siANT2 or siCTL, followed by incubation with DIC for 12
794 h. Co-immunoprecipitated protein-DNA complex was analyzed by PCR. (d)
795 Immunofluorescence analysis of C/EBPβ (green) in ASCs transfected with siANT2 (*left*
796 *panels*) or treated with genistein (Gen; 10 μM, *right panels*) in the presence of DIC for
797 12 h. Nuclei were stained with DAPI (blue). Scale bar = 50 μm. Data are expressed as
798 means ± SD (n = 3). Statistically significant differences are indicated by the
799 corresponding letters. If two groups share at least one letter between them, the difference
800 is not statistically significant. However, if two groups do not share any letter, the
801 difference between them is statistically significant. Results are representative of three
802 independent triplicate experiments. RLU: relative light unit.
803
804 Figure 7. Association of ANT2 blocking on the phosphorylation of AMPK. (a)
805 Phosphorylation of AMPK proteins in ASCs. The cells were transfected with siANT2 or
806 treated with genistein (Gen; 10 μM), followed by induction to adipocyte differentiation
807 for 7 or one day(s). (b) Western blotting of PPARγ in ASCs treated with siANT2. siRNA-
808 treated cells were induced to adipocyte differentiation in the presence or absence of
809 compound C (C.C; 1 μM). (c) Western blotting of PPARγ in ASCs treated with Gen and
810 C.C. Data are expressed as means ± SD (n = 3). Results are representative of three
811 independent triplicate experiments.
812
813 Figure 8. Blocking of AMPK restores the effect of ANT2 knockdown. (a) Transcriptional
814 activity of C/EBPs in 3T3-L1 adipocytes treated with siANT2 or siCTL. siRNA-treated
815 3T3-L1 adipocytes were transiently transfected with a pC/EBP-RE-Luc vector, followed

by induction of differentiation with compound C (C.C; 1 μM) in the presence of differentiation inducer cocktail (DIC) for 24 h. (b) ChIP analysis in ASCs treated with siANT2 (upper panels) or Gen (bottom panels), followed by induction of differentiation with C.C (1 μM) in the presence of DIC for 12 h. Co-immunoprecipitated protein-DNA complex is analyzed by PCR. Data are expressed as means ± SD (n = 3). Statistically significant differences are indicated by the corresponding letters. If two groups share at least one letter between them, the difference is not statistically significant. However, if two groups do not share any letter, the difference between them is statistically significant. Results are representative of three independent triplicate experiments. RLU: relative light unit.

Figure 1

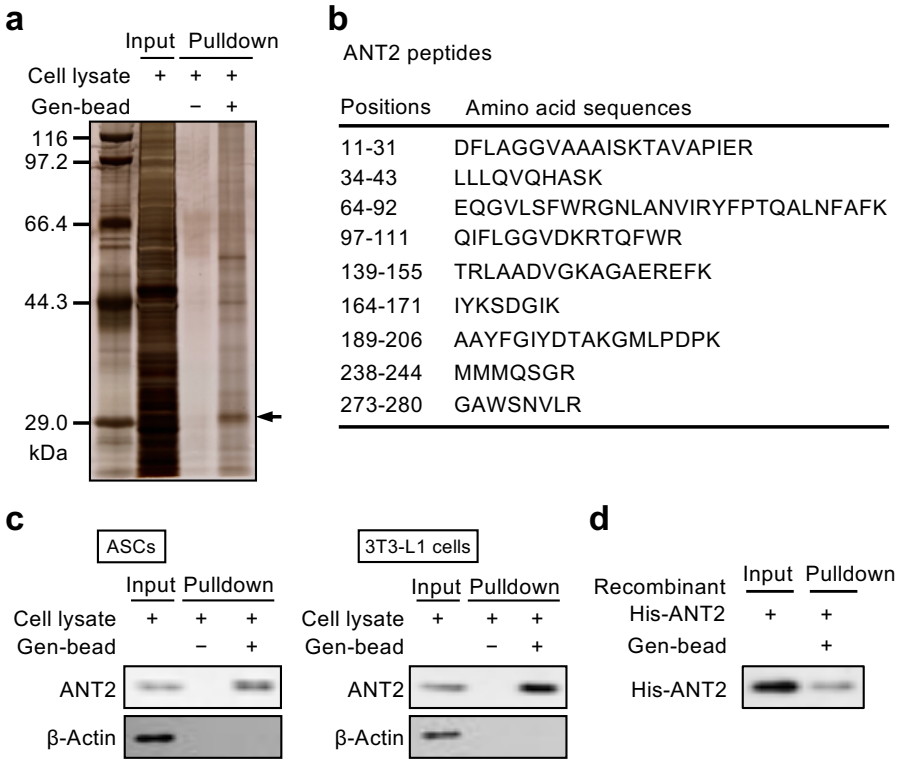
a
Input
Pulldown
Cell lysate + + +
Gen-bead − +
116
97.2
66.4
44.3
29.0
kDa
b
ANT2 peptides
Positions Amino acid sequences
11-31 DFLAGGVAAAISKTAVAPIER
34-43 LLLQVQHASK
64-92 EQGVLSFWRGNLANVIRYFPTQALNFAFK
97-111 QIFLGGVDKRTQFWR
139-155 TRLAADVGKAGAEREFK
164-171 IYKSDGIK
189-206 AAYFGIYDTAKGMLPDPK
238-244 MMMQSGR
273-280 GAWSNVLR
c
ASCs
Input Pulldown
Cell lysate + + +
Gen-bead − +
ANT2
β-Actin
3T3-L1 cells
Input Pulldown
Cell lysate + + +
Gen-bead − +
ANT2
β-Actin
d
Recombinant His-ANT2
Input Pulldown
+ +
Gen-bead +
His-ANT2

Figure 2

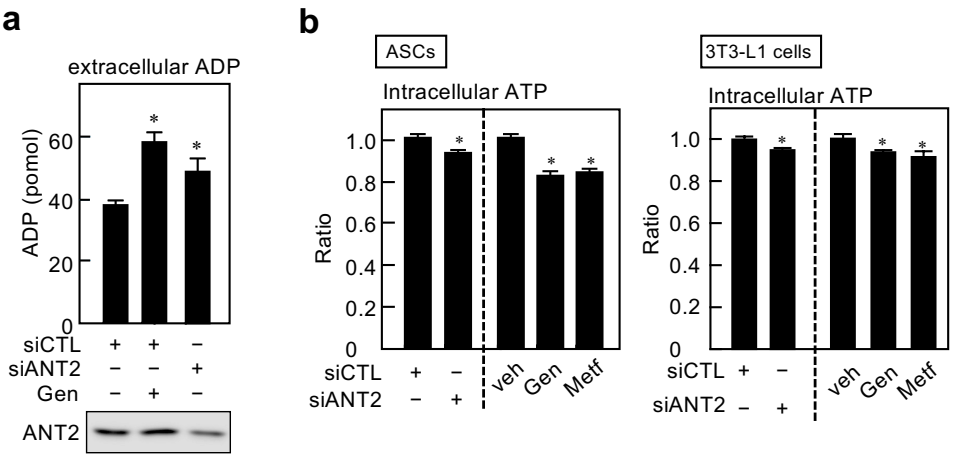
a
extracellular ADP
ADP (pomol)
60
40
20
0
siCTL + + −
siANT2 − − +
Gen − + −
ANT2
b
ASCs
Intracellular ATP
Ratio
1.0
0.8
0.6
0.4
0.2
0
siCTL + −
siANT2 − +
veh
Gen
Metf
3T3-L1 cells
Intracellular ATP
Ratio
siCTL + −
siANT2 − +
veh
Gen
Metf

Figure 3

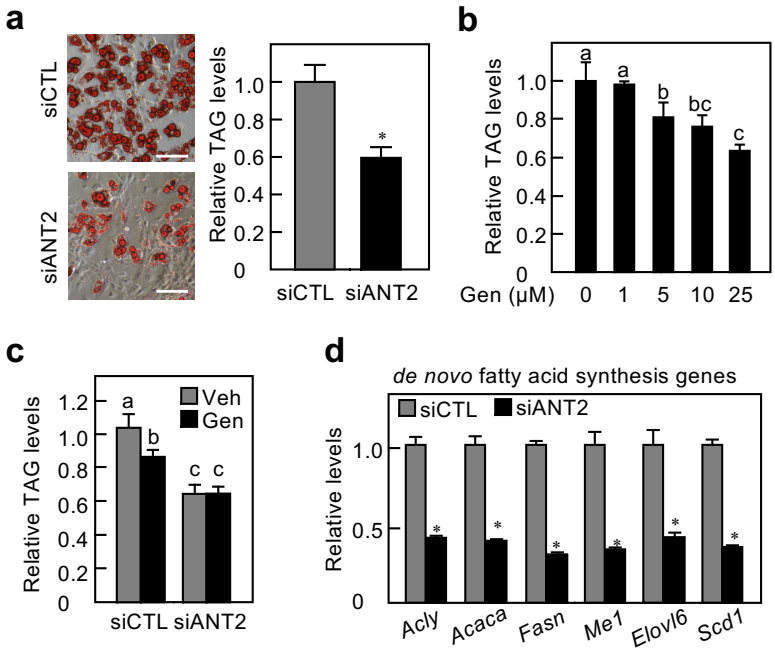
a
siCTL
siANT2
Relative TAG levels
1.0
0.8
0.6
0.4
0.2
0
siCTL siANT2
b
Relative TAG levels
a a b bc c
Gen (μM) 0 1 5 10 25
c
Relative TAG levels
Veh
Gen
a b c c
siCTL siANT2
d
de novo fatty acid synthesis genes
siCTL siANT2
Relative levels
Acly Acaca Fasn Me1 Elovl6 Scd1

Figure 4

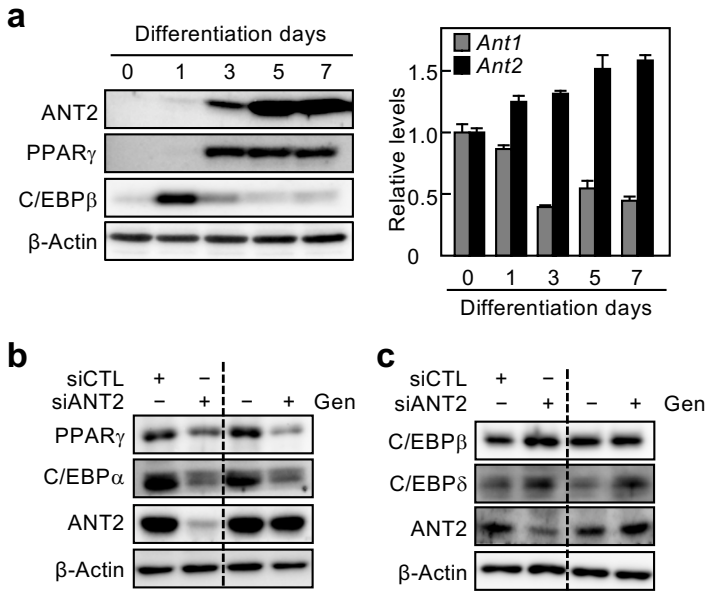
a
Differentiation days
0 1 3 5 7
ANT2
PPARγ
C/EBPβ
β-Actin
Ant1
Ant2
Relative levels
1.5
1.0
0.5
0
0 1 3 5 7
Differentiation days
b
siCTL + −
siANT2 − + − + Gen
PPARγ
C/EBPα
ANT2
β-Actin
c
siCTL + −
siANT2 − + − + Gen
C/EBPβ
C/EBPδ
ANT2
β-Actin

Figure 5

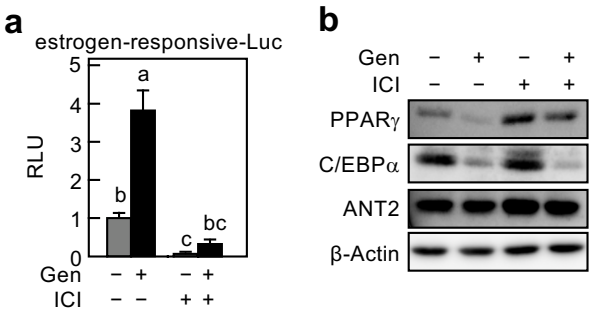
a
estrogen-responsive-Luc
RLU
5
4
3
2
1
0
a
b
c
bc
Gen − + − +
ICI − − + +
b
Gen − + − +
ICI − − + +
PPARγ
C/EBPα
ANT2
β-Actin

Figure 6

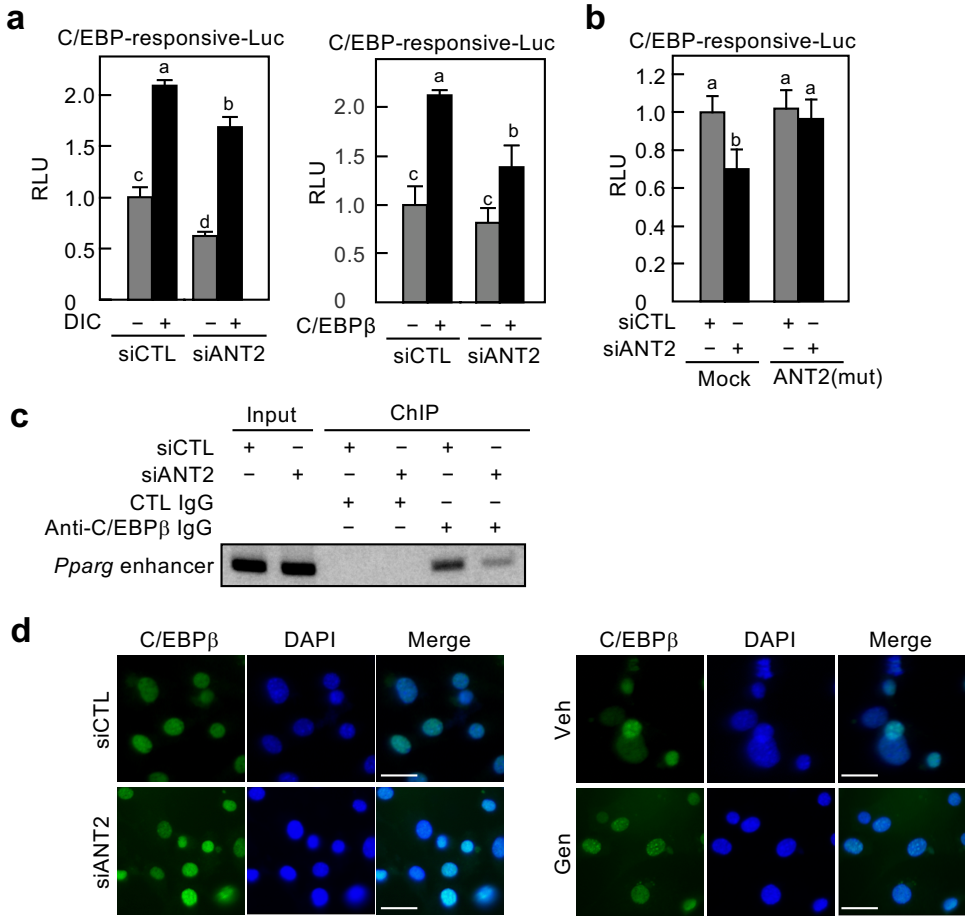
a
C/EBP-responsive-Luc
RLU
DIC
siCTL
siANT2
C/EBP-responsive-Luc
C/EBPβ
siCTL
siANT2
b
C/EBP-responsive-Luc
RLU
siCTL
siANT2
Mock
ANT2(mut)
c
Input
ChIP
siCTL
siANT2
CTL IgG
Anti-C/EBPβ IgG
Pparg enhancer
d
C/EBPβ
DAPI
Merge
siCTL
siANT2
C/EBPβ
DAPI
Merge
Veh
Gen

Figure 7

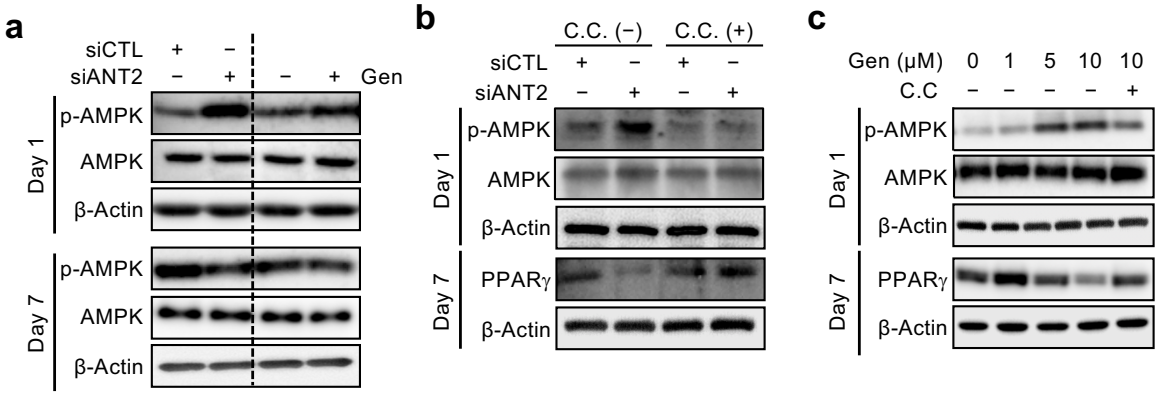
a
siCTL + − − + Gen
siANT2 − + − +
Day 1
p-AMPK
AMPK
β-Actin
Day 7
p-AMPK
AMPK
β-Actin
b
C.C. (−) C.C. (+)
siCTL + − + −
siANT2 − + − +
Day 1
p-AMPK
AMPK
β-Actin
Day 7
PPARγ
β-Actin
c
Gen (μM) 0 1 5 10 10
C.C − − − − +
Day 1
p-AMPK
AMPK
β-Actin
Day 7
PPARγ
β-Actin

Figure 8

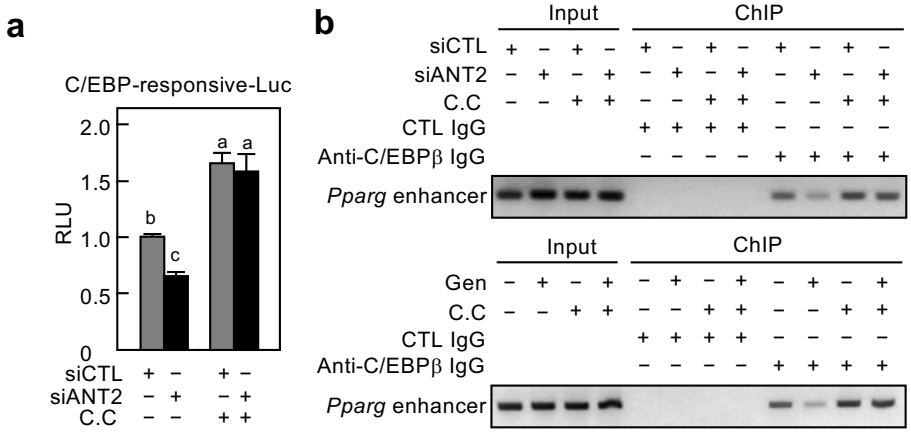
a
C/EBP-responsive-Luc
RLU
2.0
1.5
1.0
0.5
0
a
a
b
c
siCTL + − + −
siANT2 − + − +
C.C − − + +
b
Input
ChIP
siCTL + − + − + − + − + − + −
siANT2 − + − + − + − + − + − +
C.C − − + + − − + + − − + +
CTL IgG + + + + − − − −
Anti-C/EBPβ IgG − − − − + + + +
Pparg enhancer
Input
ChIP
Gen − + − + − + − + − + − +
C.C − − + + − − + + − − + +
CTL IgG + + + + − − − −
Anti-C/EBPβ IgG − − − − + + + +
Pparg enhancer

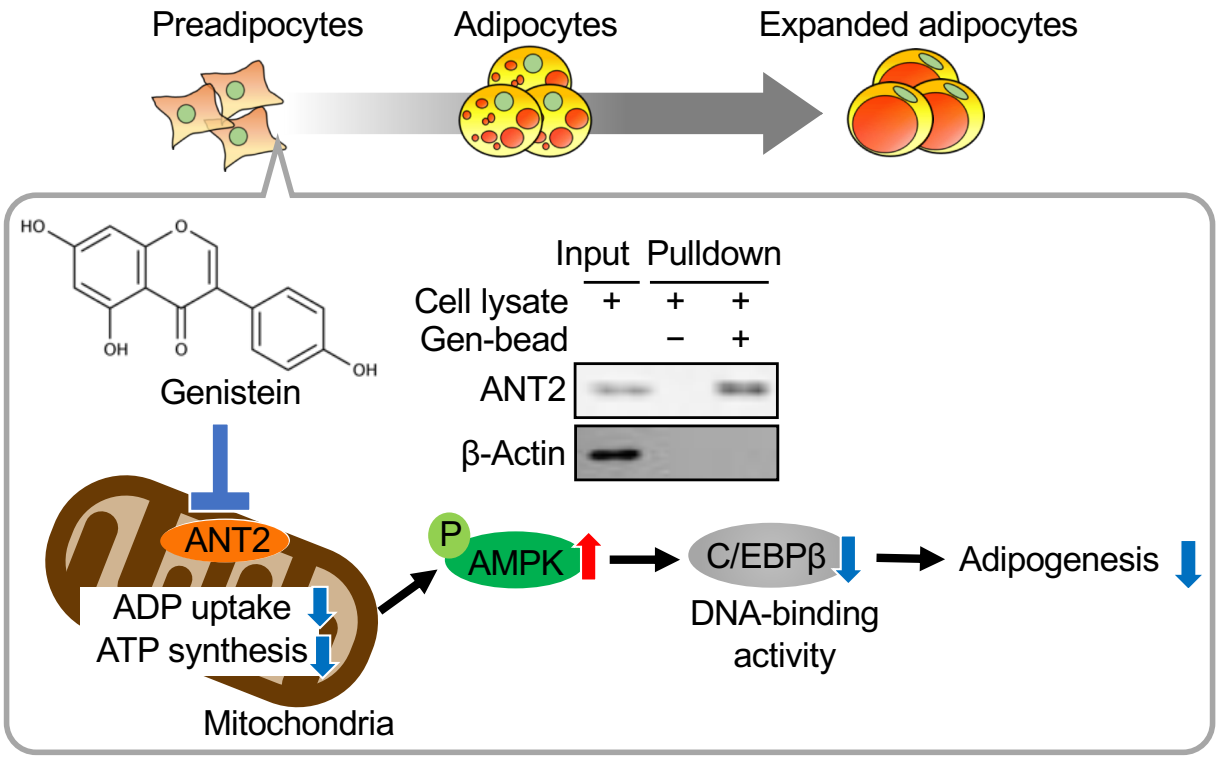
Preadipocytes
Adipocytes
Expanded adipocytes
HO
O
OH
O
OH
Genistein
Input
Pulldown
Cell lysate + + +
Gen-bead − +
ANT2
β-Actin
ANT2
ADP uptake
ATP synthesis
Mitochondria
P
AMPK
C/EBPβ
DNA-binding activity
Adipogenesis